Nanoscale Advances

ROYAL SOCIETY OF CHEMISTRY

COMMUNICATION

View Article Online
View Journal | View Issue

Cite this: *Nanoscale Adv.*, 2025, **7**, 5944

Received 25th June 2025
Accepted 11th August 2025

DOI: 10.1039/d5na00623f

rsc.li/nanoscale-advances

Carrier recombination manipulation for tunable multicolor emission in two-dimensional transition metal dichalcogenide light-emitting devices

Mi-Hsueh (Michelle) Wu,[ab] James Singh Konthoujam,[b] Iris Lin,[bc] Tzu-Yu Peng,[bd] Yu-Jung Lu[bd] and Min-Hsiung Shih[*bef]

We demonstrate a dual-colored light-emitting device using 2D semiconductors by modulating AC carrier injection through independent electrodes with phase delay, enabling balanced emission from WSe_2 and WS_2 monolayers. This innovative approach allows balanced, dynamically controllable, and spectrally stable emissions from WSe_2 and WS_2 monolayers, significantly enhancing emission control and expanding possibilities in advanced multicolor optoelectronic applications, including integrated photonic circuits and high-resolution display technologies.

Introduction

Two-dimensional (2D) materials, particularly transition metal dichalcogenides (TMDCs) such as WS_2 and WSe_2, have emerged as promising candidates for advanced optoelectronic applications, owing to their distinctive electronic and optical properties. These properties include a highly tunable bandgap that transitions from indirect in bulk form to direct in monolayer form, robust excitonic effects with large binding energies, and inherent compatibility with van der Waals heterostructures, which enables seamless integration and novel device architectures.[1–5] Such unique attributes position TMDCs as ideal materials for innovative photonic and optoelectronic devices, including LEDs, lasers, photodetectors, and quantum emitters.[6–13]

While significant progress has been made in demonstrating efficient single-color emission from monolayer TMDC devices, achieving controlled and balanced multicolor emission remains a substantial challenge. This difficulty arises primarily from intricate disparities in carrier dynamics, including differences in transport efficiency, recombination mechanisms, and the influence of interface states when combining various materials into heterostructures.[14–16] The complexity is further amplified by the interplay of excitonic phenomena, interface-induced energy transfer processes, and defect-mediated nonradiative pathways, which collectively govern the emission characteristics.[17,18]

To overcome these challenges, it is imperative to develop a deeper understanding of carrier dynamics at the nanoscale and precisely control heterointerface engineering.[19] Addressing these critical issues will pave the way toward realizing tunable, efficient, and stable multicolor emission in TMDC-based optoelectronic devices, significantly expanding their applicability in next-generation display technologies, quantum information science, and integrated photonic circuits.[20,21]

This work presents a novel dual-color electroluminescent platform based on WS_2 and WSe_2 monolayers, utilizing independently biased electrodes and phase-controlled alternating current (AC) carrier injection. By introducing a phase delay between the AC signals, we dynamically modulate charge injection into each TMDC layer, allowing for temporally separated but spectrally distinct emission. This method overcomes the intrinsic imbalance in carrier dynamics, enabling simultaneous and tunable multicolor output without the need for multiple excitation sources or spatial separation. Our architecture leverages the natural differences in transport and trapping behaviors of WS_2 and WSe_2 to engineer the emission profile. Electrical and optical measurements confirm spectrally resolved, stable dual-color emission with controllable intensity ratios, demonstrating excellent temporal stability and reproducibility. This strategy provides a scalable, fabrication-friendly solution for integrating multicolor light emission into compact optoelectronic devices.

Overall, our approach offers a powerful framework for color-tunable and energy-efficient light-emitting systems based on 2D materials. It opens new opportunities for applications in on-

[a]*Department of Electrical Engineering, Purdue University, IN 47907, USA*
[b]*Research Center for Applied Sciences (RCAS), Academia Sinica, Taipei 11529, Taiwan. E-mail: mhshih@gate.sinica.edu.tw*
[c]*Department of Electrical Engineering, University of Toronto, ON M5S 1A1, Canada*
[d]*Department of Physics, National Taiwan University, Taipei 10617, Taiwan*
[e]*Department of Photonics and Institute of Electro-Optical Engineering, National Yang Ming Chiao Tung University, Hsinchu 30010, Taiwan*
[f]*Department of Photonics, National Sun Yat-sen University, Kaohsiung 80424, Taiwan*

chip optical communication, reconfigurable display technologies, and hybrid photonic-electronic platforms.

Experimental

To investigate the impact of layer configuration on carrier injection and electroluminescent behavior in two-dimensional TMDC heterostructures, two distinct device architectures were fabricated for comparative analysis. Both devices were designed to facilitate vertical carrier injection across the TMDC interface, enabling the study of injection-direction-dependent optoelectronic characteristics. Device 1 consisted of a WS_2 monolayer as the bottom layer, with a WSe_2 monolayer transferred on top. Device 2 featured the reverse stacking order, with a WSe_2 monolayer forming the bottom layer and a WS_2 monolayer positioned above. In both architectures, Au interdigitated electrodes were deposited onto an Al_2O_3/Si substrate using thermal evaporation to form the bottom electrical contacts. The monolayers of WS_2 and WSe_2 were then sequentially transferred onto the substrate using a dry exfoliation technique under a deterministic placement scheme to ensure precise stacking and minimal interlayer contamination. This configuration allowed for efficient carrier injection through the TMDC vertical heterojunction, enabling a systematic exploration of the electroluminescent response as a function of layer ordering and interface directionality.

Results and discussion

Fig. 1 presents the schematic illustration and emission characteristics of dual-color electroluminescent devices based on vertically stacked WS_2 and WSe_2 monolayers. As shown in Fig. 1(a), the device consists of two independently biased electrodes applying phase-shifted alternating current to modulate carrier injection into the heterostructure assembled on a p^{++} silicon substrate with an Al_2O_3 dielectric layer. Fig. 1(b) compares the architectures of the two investigated devices: in Device 1, the WS_2 monolayer is positioned at the bottom, in direct contact with the Au electrode, enabling carrier injection through WS_2, whereas in Device 2, the WSe_2 monolayer is placed at the bottom, resulting in carrier injection through WSe_2. Fig. 1(c) displays the corresponding electroluminescence (EL) spectra from both devices, showing distinct peaks associated with WS_2 and WSe_2 emissions. Device 1 exhibits balanced dual-color emission with comparable intensities from both monolayers, while Device 2 shows a significant disparity, with dominant WSe_2 emission. The origins of this stark difference in emission behavior, particularly related to the differences in carrier transport dynamics and trapping effects in the monolayers, are further explored in the following section.

In order to better understand the stark contrast in emission behavior observed between Device 1 and Device 2 in Fig. 1, we investigated the carrier transport characteristics of individual WS_2 and WSe_2 monolayers by measuring their transfer curves (I_d–V_g) under identical conditions, as shown in Fig. 2(a) and (b), respectively. The WS_2-based FET exhibits minimal hysteresis between the forward and reverse gate-voltage sweeps, indicating negligible carrier trapping phenomena and suggesting efficient carrier transport within the WS_2 monolayer. Conversely, the WSe_2-based FET displays pronounced hysteresis, characterized by a significant divergence between the forward and reverse sweeps. This behavior clearly indicates substantial carrier trapping effects in the WSe_2 monolayer, which substantially influences its transport dynamics.

Electrical measurements further elucidated these carrier transport behaviors by comparing the transfer characteristics of

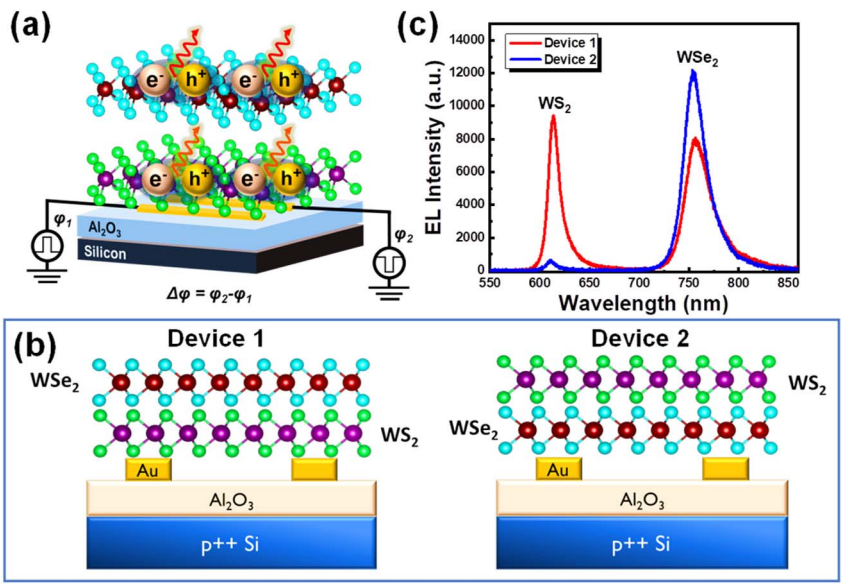

Fig. 1 (a) Schematic illustration of the dual-color electroluminescent device utilizing stacked monolayers of WS_2 and WSe_2 with independent AC-driven electrodes. (b) Cross-sectional schematics of Device 1 and Device 2. (c) EL spectra for both devices, showing emission from WS_2 and WSe_2.

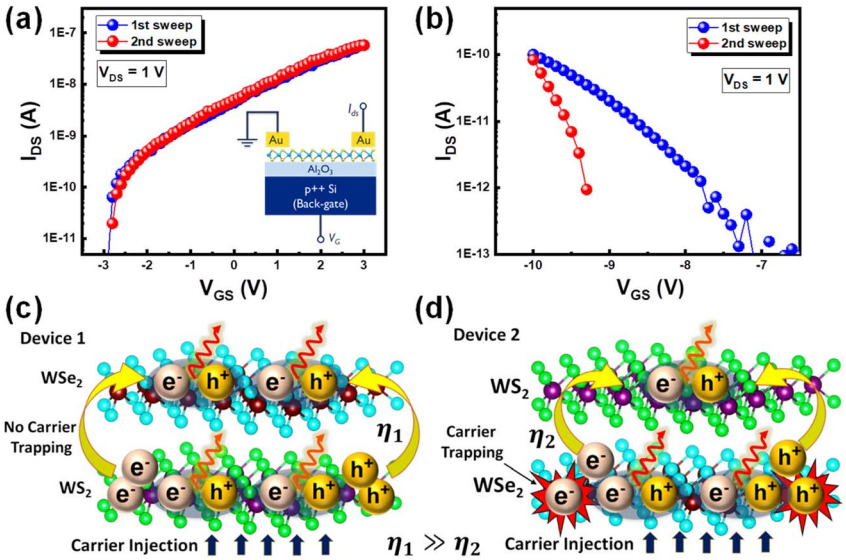

Fig. 2 Transfer characteristics for (a) WS_2 FET; inset: FET device structure. (b) WSe_2 FET. (c and d) Schematic representations of carrier injection and recombination processes in Device 1 and Device 2.

WS_2 and WSe_2 monolayer field-effect transistors (FETs). WS_2 demonstrated minimal hysteresis between forward and reverse gate sweeps and a relatively high field-effect mobility ($\mu = 5.29 \times 10^{-1}$ cm^2 V^{-1} s^{-1}), indicating efficient carrier transport with negligible trapping. The high carrier mobility in WS_2 arises from its favorable electronic band structure specifically, a lighter electron effective mass and steeper conduction band curvature, which facilitates faster carrier transport. Additionally, WS_2 exhibits weaker electron–phonon scattering and a lower intrinsic defect density due to its high sulfur vacancy formation energy (~3.38 eV), which minimizes impurity-induced scattering.[22] In contrast, WSe_2 shows heavier effective masses and higher defect densities that introduce deep trap states, degrading mobility. Additionally, the subthreshold swing (SS) for WS_2 was extracted to be approximately 498 mV dec^{-1}, suggesting strong gate control and low interface state density. In contrast, the WSe_2 FET exhibited pronounced hysteresis and a significantly lower mobility ($\mu = 1.09 \times 10^{-3}$ cm^2 V^{-1} s^{-1}), accompanied by a higher SS value approximately 873 mV dec^{-1}. This large SS reflects poor electrostatic control and a high density of trap states near the channel–dielectric interface, leading to sluggish carrier response and pronounced trapping. These contrasting transport metrics—namely, higher mobility and lower SS in WS_2 *versus* poor mobility and high SS in WSe_2—directly affect the charge injection, transport, and recombination dynamics in the electroluminescent devices.

These contrasting transport behaviors have direct implications for carrier injection and recombination in the dual-color electroluminescent devices described previously. To further illustrate how these transport characteristics directly influence the observed emission behavior, Fig. 2(c) and (d) provide schematic representations of carrier transport and recombination dynamics within Device 1 and Device 2, respectively. In Device 1 (Fig. 2(c)), carriers injected into the WS_2 monolayer easily transport to the adjacent WSe_2 monolayer due to the negligible trapping effects. However, for Device 2 (Fig. 2(d)), the pronounced trapping in WSe_2 significantly restricts carrier transport into the WS_2 monolayer, effectively limiting radiative recombination in WS_2. Specifically, the negligible carrier trapping and superior mobility in WS_2 facilitate efficient carrier injection and transport through this monolayer, thereby effectively supplying carriers to both WS_2 and adjacent WSe_2 layers for radiative recombination in Device 1. The pronounced charge trapping observed in the WSe_2 layer, as compared to WS_2, arises predominantly from intrinsic differences in defect chemistry between the two materials. Specifically, WSe_2 inherently exhibits a higher density of Se vacancies, which introduce deep mid-gap states that act as efficient electron traps. These trap states significantly hinder charge transport and recombination dynamics, often manifesting as strong hysteresis and reduced electroluminescence efficiency. Experimental and theoretical investigations have demonstrated that the vacancy formation energy for WSe_2 is relatively low (~2.81 eV), which facilitates spontaneous defect formation and contributes to the high density of deep trap states.[22,23] In contrast, WS_2 exhibits a more defect-tolerant behavior due to its higher sulfur vacancy formation energy (~3.38 eV), which suppresses the formation of deep-level defects. The resulting shallow trap states, located closer to the band edges, can more readily release captured charges and thus exhibit reduced charge trapping and hysteresis.[22] Consequently, Device 1 demonstrates balanced emission intensities from both WS_2 and WSe_2 monolayers. In contrast, the pronounced trapping effect in the WSe_2 monolayer hinders efficient carrier transport when carriers are directly injected through WSe_2 (Device 2). This limitation restricts the availability of carriers to reach the WS_2 layer, resulting in significantly imbalanced emission intensities with dominant emission from WSe_2. These results clearly highlight the critical

role of carrier transport and trapping mechanisms in determining the emission performance of dual-color electroluminescent devices based on stacked 2D semiconductor monolayers.

To further validate the role of phase-controlled carrier injection in achieving balanced dual-color emission, we systematically investigated the effect of phase delay and duty cycle on the electroluminescence (EL) intensity of WS_2 and WSe_2 monolayers in both Device 1 and Device 2, as shown in Fig. 3. For Device 1 (Fig. 3(a)), the EL peak intensities of WS_2 and WSe_2 were recorded while varying the phase delay (top panel) and the duty cycle (bottom panel) of the AC driving signals applied to the injection electrodes. A pronounced dependence of EL emission on both parameters was observed, confirming their critical influence on the temporal dynamics of carrier injection and recombination.

Notably, when the phase delay was set to 150° and the duty cycle to 60%, the emission intensities from WS_2 and WSe_2 converged—marked by the ellipses—indicating a condition of balanced carrier injection into both monolayers. This balance results from an optimal overlap in the temporal profiles of electron and hole injection, leading to efficient and simultaneous radiative recombination in both WS_2 and WSe_2. These results highlight the importance of synchronizing the injection phases to control interlayer carrier distribution and recombination behavior.

Interestingly, a significant difference in EL intensities is observed at a phase delay of 180° and a duty cycle of 40%, where WS_2 emission becomes dominant over WSe_2. Because of the type-II alignment, injected electrons and holes tend to remain in different layers, suppressing intralayer recombination.[24,25] However, the timing of 180° pulsing can transiently co-locate carriers. For example, consider a half-cycle when electrons have built up in WS_2 from the previous pulse: when the phase flips, holes are injected into WS_2 (*via* the opposite electrode). These co-located electrons and holes in WS_2 can form a bright intralayer exciton, which radiatively recombines quickly. Conversely, when holes accumulate in WSe_2 and electrons are injected into WSe_2, those electrons will almost immediately transfer to WS_2 rather than recombine in WSe_2. Thus, WSe_2 almost never has both carriers simultaneously, and its intralayer emission stays weak and roughly constant. In summary, the 180° drive favors intralayer WS_2 exciton emission: electrons spend most time in WS_2 and meet holes there only under time-shifted injection. The observed pronounced intensity at the specific duty cycle (40%) results from optimal temporal carrier overlap, minimizing non-radiative recombination channels such as Auger processes and exciton–exciton annihilation that occur prominently at higher duty cycles. Lower duty cycles limit the build-up of excessive carrier densities, while longer duty cycles tend to enhance non-radiative recombination processes, thus reducing emission efficiency. The error bars represent the standard deviation across different multiple devices and the relatively

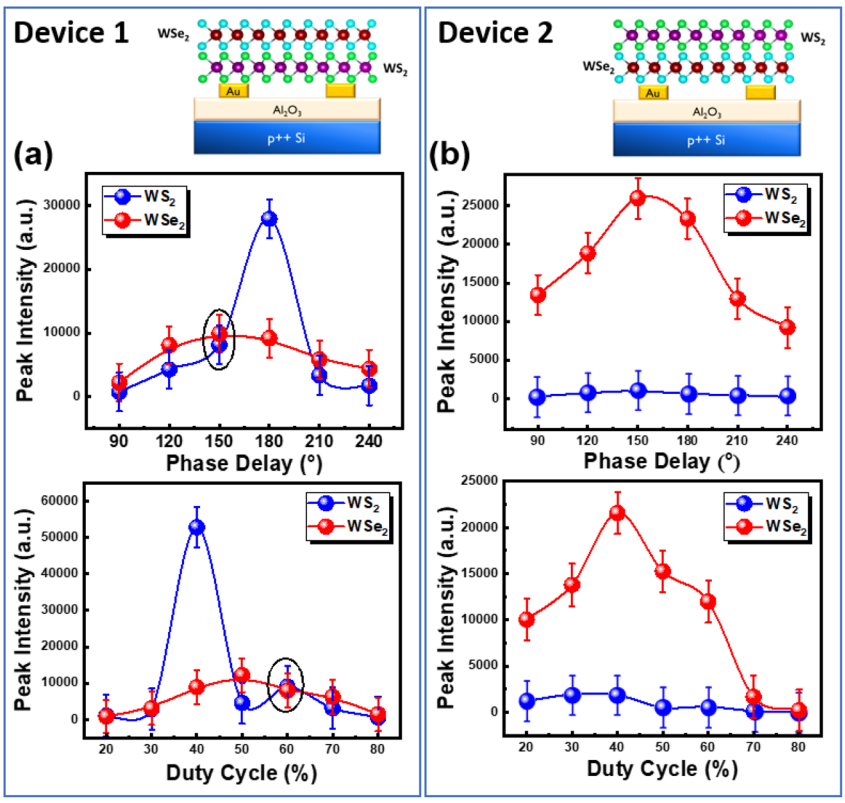

Fig. 3 EL peak intensity of WS_2 and WSe_2 as a function of phase delay (top) and duty cycle (bottom) for Device 1 (a) and Device 2 (b), highlighting tunable and balanced emission in Device 1 and persistent imbalance in Device 2. Error bars represent the standard deviation.

small deviations observed confirm that the trends—such as balanced emission at optimal phase delay and duty cycle in Device 1, and persistent imbalance in Device 2—are highly reproducible.

In Device 2 (Fig. 4(b)), however, such tunability is absent. The emission from WSe_2 varies modestly with changes in phase delay and duty cycle, but the EL intensity from WS_2 remains consistently low across all conditions. This further emphasizes the impact of carrier trapping in WSe_2, which obstructs the flow of carriers to the WS_2 layer and limits recombination there, regardless of the injection timing. Thus, while Device 1 demonstrates highly tunable and balanced dual-color operation through carrier injection engineering, Device 2 remains constrained by material-induced transport asymmetries. These findings clearly demonstrate the necessity of understanding and leveraging monolayer-specific carrier dynamics when designing phase-controlled multicolor 2D optoelectronic systems.

To evaluate the spectral stability of the dual-color electroluminescence (EL) under dynamic injection conditions, we analyzed the peak emission wavelengths of WS_2 and WSe_2 as functions of both phase delay and duty cycle, as shown in Fig. 4(a) and (b). The left panel of the figure presents the emission peak positions of WS_2 (blue) and WSe_2 (red) as the phase delay between the dual-pulse inputs is varied from 90° to 240°, while the right panel depicts the same under varying duty cycles ranging from 20% to 80%. In both cases, the emission peaks for WS_2 and WSe_2 remain spectrally invariant—centered at approximately 625 nm and 750 nm, respectively—regardless of the modulation parameter. To gain further insight into the nature of the light emission, we considered the possible recombination pathways in our dual-color electroluminescent devices. The emission spectra of both WS_2 and WSe_2 monolayers show sharp and spectrally stable peaks centered around ~625 nm and ~750 nm, respectively, consistent with the A-exciton transitions of these monolayers.[12,26] This spectral signature indicates that the dominant recombination mechanism is radiative recombination of neutral excitons, rather than defect-related states or trion complexes. Nevertheless, non-radiative recombination pathways, such as trap-assisted recombination, are likely present, especially in the WSe_2 monolayer, which exhibits stronger hysteresis and higher subthreshold swing in FET measurements—indicative of a high density of localized trap states. These traps can capture carriers and hinder their recombination, leading to the observed imbalance in emission intensity, particularly when carrier injection occurs through WSe_2. Overall, the dominant emission mechanism in our system is excitonic radiative recombination, modulated by the transport and trapping characteristics of each monolayer. Minimizing non-radiative recombination *via* improved interface engineering or chemical passivation could further enhance the quantum efficiency of these 2D electroluminescent devices.

This spectral constancy across all modulation regimes indicates that the applied electrical modulation influences only the carrier recombination dynamics and temporal emission intensities, without affecting the intrinsic band structure or excitonic transition energies of either monolayer. Such robustness is critical for applications where consistent color output is essential, including multicolor displays and spectrally stable light sources. To quantitatively evaluate the tunable emission behavior, we mapped the electroluminescence spectra under varying phase delays and duty cycles onto the CIE 1931 chromaticity diagram (Fig. S1). The resulting color coordinates demonstrate a clear trajectory across the red-orange region, governed by the relative contributions of WS_2 (~625 nm) and WSe_2 (~750 nm) emission. This tunable color mixing, achieved through electrical control alone, highlights the potential of our device architecture for integrated multicolor light sources and next-generation display technologies, where dynamic and pixel-level color modulation is essential. These results confirm that the employed modulation strategy allows for tunable intensity control while maintaining high spectral fidelity, which is crucial for reliable and predictable performance in integrated optoelectronic and visible light communication systems. Beyond the demonstrated WS_2 and WSe_2 system, the proposed phase-controlled AC carrier injection strategy is broadly extendable to other 2D semiconductors with diverse bandgaps. In particular, wide-bandgap layered materials such as GaS, GaSe, InSe, SnS_2, GeS_2, and PbI_2 have been experimentally demonstrated to emit in the green and blue spectral regions.[27] These materials, with their atomically thin structures and strong excitonic effects, represent promising candidates for achieving short-wavelength electroluminescence in future implementations of

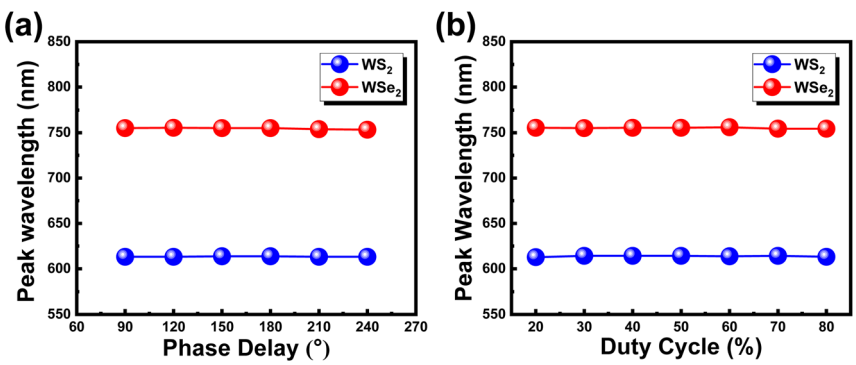

Fig. 4 Spectral stability for the dual-color EL device (a) phase delay dependent and (b) duty cycle dependent.

this platform. Moreover, the availability of Ruddlesden–Popper 2D perovskites and transition metal oxides (*e.g.*, MoO_3, V_2O_5) further broadens the accessible color gamut towards the blue-violet region.[27] The success of our device relies on engineering the carrier injection dynamics and leveraging differential transport characteristics, which can also be applied to these wide-bandgap systems, provided that their electronic properties—such as mobility and trap state density—are suitably tailored. This generality enables the design of electrically tunable multicolor or even full-spectrum 2D light-emitting devices, paving the way for advanced on-chip photonic systems, spectrally reconfigurable displays, and visible light communication technologies.

Conclusions

We developed a dual-color electroluminescent device based on vertically stacked WS_2/WSe_2 monolayers using phase-controlled AC carrier injection. By injecting carriers through the WS_2 layer (Device 1), we achieved tunable and balanced emission intensities through optimization of phase delay (150°) and duty cycle (60%). In contrast, Device 2, with injection through WSe_2, showed consistently imbalanced emission due to significant carrier trapping. Electrical measurements confirmed that WS_2 exhibits higher mobility (5.29×10^{-1} cm^2 V^{-1} s^{-1}) compared to WSe_2 (1.09×10^{-3} cm^2 V^{-1} s^{-1}). Additionally, the emission wavelengths remained stable across all injection conditions, confirming the spectral robustness of the device. This strategy demonstrates an effective route for realizing tunable, spectrally stable multicolor emission in 2D optoelectronic systems.

Conflicts of interest

There are no conflicts to declare.

Data availability

The data that support the findings of this study are available from the corresponding author, upon reasonable request.

Color chromaticity diagram for the devices. See DOI: **https://doi.org/10.1039/d5na00623f**.

References

1 P.-L. Chen, T. Ahmed, C. Kuo, C.-C. Lu, D.-H. Lien and C.-H. Liu, Emerging 2D Materials and Van der Waals Heterostructures for Advanced NIR, SWIR, and MWIR Emitters, *Small Methods*, 2024, 2401550.
2 A. K. Geim and I. V. Grigorieva, Van der Waals heterostructures, *Nature*, 2013, **499**(7459), 419–425.
3 C. Gong, Y. Zhang, W. Chen, J. Chu, T. Lei, J. Pu, L. Dai, C. Wu, Y. Cheng, T. Zhai, L. Li and J. Xiong, Electronic and Optoelectronic Applications Based on 2D Novel Anisotropic Transition Metal Dichalcogenides, *Advanced Science*, 2017, **4**(12), 1700231.
4 K. F. Mak and J. Shan, Photonics and optoelectronics of 2D semiconductor transition metal dichalcogenides, *Nat. Photonics*, 2016, **10**(4), 216–226.
5 J. Wang, I. Verzhbitskiy and G. Eda, Electroluminescent Devices Based on 2D Semiconducting Transition Metal Dichalcogenides, *Adv. Mater.*, 2018, **30**(47), 1802687.
6 T. Ahmed, J. Zha, K. K. H. Lin, H.-C. Kuo, C. Tan and D.-H. Lien, Bright and Efficient Light-Emitting Devices Based on 2D Transition Metal Dichalcogenides, *Adv. Mater.*, 2023, **35**(31), 2208054.
7 I. Barth, M. Deckart, D. Conteduca, G. S. Arruda, Z. Hayran, S. Pasko, S. Krotkus, M. Heuken, F. Monticone, T. F. Krauss, E. R. Martins and Y. Wang, Lasing from a Large-Area 2D Material Enabled by a Dual-Resonance Metasurface, *ACS Nano*, 2024, **18**(20), 12897–12904.
8 Y.-H. Chang, Y.-S. Lin, K. James Singh, H.-T. Lin, C.-Y. Chang, Z.-Z. Chen, Y.-W. Zhang, S.-Y. Lin, H.-C. Kuo and M.-H. Shih, AC-driven multicolor electroluminescence from a hybrid WSe2 monolayer/AlGaInP quantum well light-emitting device, *Nanoscale*, 2023, **15**(3), 1347–1356.
9 C. Frydendahl, T. Yezekyan, V. A. Zenin and S. I. Bozhevolnyi, 2D Semiconductors as On-Chip Light Sources for Integrated Nanophotonics, *Nano Lett.*, 2025, **25**(16), 6414–6420.
10 J. S. Konthoujam, Y.-S. Lin, Y.-H. Chang, H.-T. Lin, C.-Y. Chang, Y.-W. Zhang, S.-Y. Lin, H.-C. Kuo and M.-H. Shih, Dynamical characteristics of AC-driven hybrid WSe2 monolayer/AlGaInP quantum wells light-emitting device, *Discover Nano*, 2023, **18**(1), 140.
11 J. S. Konthoujam, Y.-S. Lin, Z.-Z. Chen, C.-Y. Chang, Y.-W. Zhang, S.-Y. Lin, D.-H. Lien, H.-C. Kuo and M.-H. Shih, Electrical Control of Electroluminescence in 2D Semiconductor Light Emitting Device through Synchronous Injection of Electrons and Holes, *Adv. Mater. Technol.*, 2025, **10**(7), 2401743.
12 J. S. Konthoujam, P.-J. Pu, C.-J. Chang, S.-Y. Lin, K.-B. Lin, C.-C. Kaun and M.-H. Shih, Van der Waals Contact Induced Defect States-Free Interface for Boosting Electroluminescence in 2D Semiconductor Light Emitting Device, *Adv. Mater. Technol.*, 2025, e00268.
13 A. Rani, A. Verma and B. C. Yadav, Advancements in transition metal dichalcogenides (TMDCs) for self-powered photodetectors: challenges, properties, and functionalization strategies, *Mater. Adv.*, 2024, **5**(9), 3535–3562.
14 D. D. Blach, D. B. Sulas-Kern, B. Wang, R. Long, Q. Ma, O. V. Prezhdo, J. L. Blackburn and L. Huang, Long-Range Charge Transport Facilitated by Electron Delocalization in MoS_2 and Carbon Nanotube Heterostructures, *ACS Nano*, 2025, **19**(3), 3439–3447.
15 Z. Hu, X. Liu, P. L. Hernández-Martínez, S. Zhang, P. Gu, W. Du, W. Xu, H. V. Demir, H. Liu and Q. Xiong, Interfacial charge and energy transfer in van der Waals heterojunctions, *InfoMat*, 2022, **4**(3), e12290.
16 R. Perea-Causin, D. Erkensten, J. M. Fitzgerald, J. J. P. Thompson, R. Rosati, S. Brem and E. Malic, Exciton optics, dynamics, and transport in atomically thin semiconductors, *APL Mater.*, 2022, **10**(10), 100701.

17 M. Amani, D.-H. Lien, D. Kiriya, J. Xiao, A. Azcatl, J. Noh, S. R. Madhvapathy, R. Addou, S. Kc, M. Dubey, K. Cho, R. M. Wallace, S.-C. Lee, J.-H. He, J. W. Ager, X. Zhang, E. Yablonovitch and A. Javey, Near-unity photoluminescence quantum yield in MoS2, *Science*, 2015, **350**(6264), 1065–1068.

18 L. Yuan and L. Huang, Exciton dynamics and annihilation in WS2 2D semiconductors, *Nanoscale*, 2015, **7**(16), 7402–7408.

19 J. Li, R. Yang, R. Li and C. P. Grigoropoulos, Exciton Dynamics in 2D Transition Metal Dichalcogenides, *Adv. Opt. Mater.*, 2025, **13**(11), 2403137.

20 K. Parto, S. I. Azzam, N. Lewis, S. D. Patel, S. Umezawa, K. Watanabe, T. Taniguchi and G. Moody, Cavity-Enhanced 2D Material Quantum Emitters Deterministically Integrated with Silicon Nitride Microresonators, *Nano Lett.*, 2022, **22**(23), 9748–9756.

21 J. Wu, H. Ma, P. Yin, Y. Ge, Y. Zhang, L. Li, H. Zhang and H. Lin, Two-Dimensional Materials for Integrated Photonics: Recent Advances and Future Challenges, *Small Sci.*, 2021, **1**(4), 2000053.

22 Y. Guo, D. Liu and J. Robertson, Chalcogen vacancies in monolayer transition metal dichalcogenides and Fermi level pinning at contacts, *Appl. Phys. Lett.*, 2015, **106**(17), 173106.

23 A. Schwarz, H. Alon-Yehezkel, A. Levi, R. K. Yadav, K. Majhi, Y. Tzuriel, L. Hoang, C. S. Bailey, T. Brumme, A. J. Mannix, H. Cohen, E. Yalon, T. Heine, E. Pop, O. Cheshnovsky and D. Naveh, Thiol-based defect healing of WSe2 and WS2, *npj 2D Mater. Appl.*, 2023, **7**(1), 59.

24 A. Bian, S. Liu, X. Zhang, Z. Liu, D. He, H. Zhao and J. Dai, Layer-engineered interlayer charge transfer in WSe2/WS2 heterostructures, *J. Phys. D: Appl. Phys.*, 2023, **56**(13), 135102.

25 S. Miao, T. Wang, X. Huang, D. Chen, Z. Lian, C. Wang, M. Blei, T. Taniguchi, K. Watanabe, S. Tongay, Z. Wang, D. Xiao, Y.-T. Cui and S.-F. Shi, Strong interaction between interlayer excitons and correlated electrons in WSe2/WS2 moiré superlattice, *Nat. Commun.*, 2021, **12**(1), 3608.

26 Y. Sheng, T. Chen, Y. Lu, R.-J. Chang, S. Sinha and J. H. Warner, High-Performance WS2 Monolayer Light-Emitting Tunneling Devices Using 2D Materials Grown by Chemical Vapor Deposition, *ACS Nano*, 2019, **13**(4), 4530–4537.

27 Y. Lu and J. H. Warner, Synthesis and Applications of Wide Bandgap 2D Layered Semiconductors Reaching the Green and Blue Wavelengths, *ACS Appl. Electron. Mater.*, 2020, **2**(7), 1777–1814.